Cent. Eur. J. Phys. • 6(3) • 2008 • 593-602
DOI: 10.2478/s11534-008-0047-8

VERSITA

Central European Journal of **Physics**

Shaping and switching of polychromatic light in arrays of periodically curved nonlinear waveguides*

Research Article

Ivan L. Garanovich, Andrey A. Sukhorukov, Yuri S. Kivshar†

Nonlinear Physics Centre and Centre for Ultra-high bandwidth Devices for Optical Systems (CUDOS), Research School of Physical Sciences and Engineering, Australian National University, Canberra, ACT 0200, Australia

Received 13 November 2007; accepted 11 February 2008

Abstract: We overview our recent theoretical results on spatio-spectral control, diffraction management, and broadband all-optical switching of polychromatic light in periodically curved one and two dimensional arrays of coupled optical waveguides. In particular, we show that polychromatic light beams and patterns produced by *white-light* and *supercontinuum* sources can experience *wavelength-independent* normal, anomalous, or zero diffraction in specially designed structures. We also demonstrate that in the nonlinear regime, it is possible to achieve *broadband all-optical switching* of polychromatic light in a directional waveguide coupler with special bending of the waveguide axes. Our results suggest novel opportunities for creation of all-optical logical gates and switches which can operate in a very broad frequency region, e.g., covering the *entire visible* spectrum.

PACS (2008): 42.82.Et, 42.25.Fx, 42.65.Jx, 42.65.Tg

Keywords: diffraction management • all-optical switching • polychromatic light • photonic lattices • supercontinuum

© *Versita Warsaw and Springer-Verlag Berlin Heidelberg.*

1. Introduction

Flexible shaping and steering of optical beams can be realized in periodic photonic structures, where the fundamental aspects of light propagation such as the beam diffraction and refraction can be engineered to suit specific application requirements [1, 2]. In particular, the natural tendency of beams to broaden during propagation can be controlled through diffraction management [3, 4]. Diffraction can be eliminated in periodic structures leading to self-collimation effect where the average beam width does not change over hundreds of free-space diffraction lengths [5]. On the other hand, diffraction can be made negative allowing for focusing of diverging beams [6] and imaging of objects with sub-wavelength resolution [7, 8].

Advances in the generation of light with broadband or supercontinuum spectrum in photonic-crystal fibers [9–11] open many new possibilities for a wide range of applications including optical frequency metrology [12], spectroscopy [13], tomography [14], and optical characterization of photonic crystals [15]. However, extended photonic structures are primarily optimized for beam shaping and deflection in a narrow-frequency range. Indeed, the physics of periodic structures is governed by scattering of waves from modulations of the refractive index and

*Presented at 9-th International Workshop on Nonlinear Optics Applications, NOA 2007, May 17-20, 2007, Świnoujście, Poland

†E-mail: ilg124@rsphysse.anu.edu.au

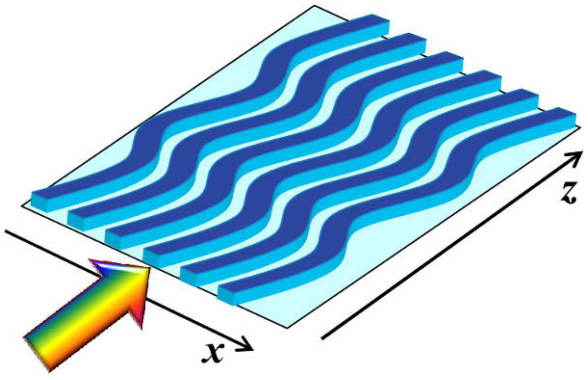


Figure 1. Schematic drawing of a curved waveguide array composed of the periodically bended waveguides.

their subsequent interference. This is a resonant process, which is sensitive to both the frequency and propagation angle. Strong dependence of the beam refraction on the optical wavelength known as *superprism effect* was observed in photonic crystals [16]. Spatial beam diffraction also depends on the wavelength; for example it was found in recent experiments [5, 17] that the effect of beam self-collimation through diffraction cancellation was restricted to a spectral range of less than 10% of the central frequency. Such a strong dependence of the spatial beam dynamics on wavelength can be used for multiplexing and demultiplexing of signals in optical communication networks [18, 19]. On the other hand, it is important to explore the potential of periodic photonic structures for tunable spatial shaping of the polychromatic light beams.

In this paper, we overview our recent theoretical results [20–22] on shaping and switching of polychromatic light beams in arrays of coupled optical waveguides, which axes are periodically curved in the propagation direction as schematically shown in Fig. 1. In particular, we show that intrinsic wavelength-dependence of diffraction strength in periodic systems can be compensated by geometrically-induced dispersion and introduce the concept of *wavelength-independent diffraction management* in a very broad frequency range covering a spectral range up to 50% of the central frequency. This opens up novel opportunities for efficient self-collimation, focusing, and shaping of white-light beams and patterns. We also demonstrate that in the nonlinear regime, it is possible to achieve *broadband all-optical switching* of polychromatic light in a directional waveguide coupler with special bending of the waveguide axes. Our results suggest new opportunities for all-optical control of polychromatic light, offering additional flexibility compared to the spatial-spectral reshaping recently demonstrated experimentally in arrays of straight optical waveguides [23–25].

The paper is organized as follows. In Sec. 2 we present the basic concepts of polychromatic light propagation in periodically curved waveguide arrays at low light intensity (linear propagation) and introduce the concept of broadband diffraction management in modulated lattices. In Sec. 3 and Sec. 4 we describe how to design modulated lattices optimized for broadband diffraction cancellation, and wavelength-independent normal or anomalous diffraction, respectively. We then show how these structures can be used to realize multicolor discrete Talbot effect for polychromatic light patterns in Sec. 5. Sec. 6 describes the nonlinear polychromatic coupler designed for collective all-optical switching of frequency components in a very broad spectral region. Finally, in Sec. 7 we briefly describe novel opportunities for spatio-spectral shaping of supercontinuum radiation in two-dimensional modulated photonic lattices.

2. Light propagation in periodically curved waveguide arrays

We study propagation of beams emitted by a continuous white-light source in a periodic array of coupled optical waveguides, where the waveguide axes are periodically curved in the propagation direction z, as it is schematically shown in Fig. 1(a). Such waveguide array structures can be created using established fabrication techniques [3, 17, 26–29].

In media with slow nonlinear response, where the coherent four-wave-mixing processes are suppressed and optically-induced refractive index change is defined by the time-averaged light intensity of different spectral components [30, 31], the overall beam dynamics is governed by the set of normalized paraxial equations for the complex beam envelopes $E(x,z;\lambda)$ at vacuum wavelengths λ_m,

$$i\frac{\partial E_m}{\partial z}+\frac{z_s\lambda_m}{4\pi n_0 x_s^2}\frac{\partial^2 E_m}{\partial x^2}+\frac{2\pi z_s}{\lambda_m}\left\{v\left[x-x_0(z)\right]+\mathcal{G}\right\}E_m=0, \tag{1}$$

where x and z are the transverse and propagation coordinates normalized to the characteristic values $x_s = 1$ μm and $z_s = 1$ mm, respectively, c is the speed of light, n_0 is the average refractive index of the medium, $v(x) \equiv v(x+d)$ is the transverse refractive index profile of the waveguide array with the transverse period d, longitudinal bending profile of the waveguide axis $x_0(z) \equiv x_0(z+L)$ defines the periodic longitudinal lattice modulation with the period $L \gg d$, $\mathcal{G} = \alpha M^{-1}\sum_{m=1}^{M}\gamma(\lambda_m)|E_m|^2$ defines nonlinear change of refractive index, α is the nonlinear coefficient, and $\gamma(\lambda)$ accounts for dispersion of the nonlinear response. In numerical simulations, we choose a large number of

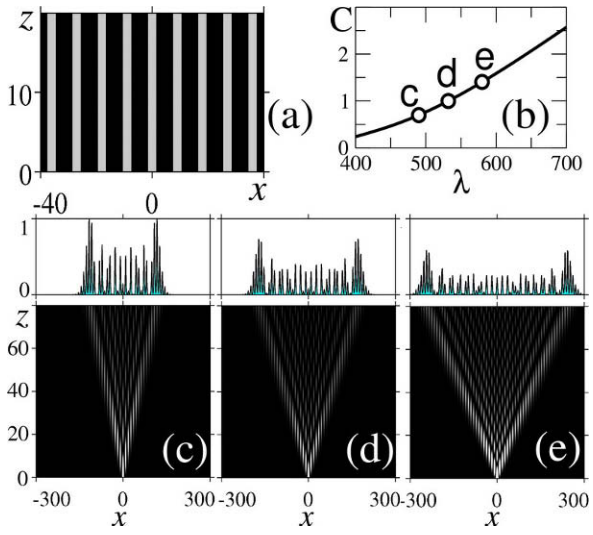


Figure 2. Discrete diffraction in (a) straight waveguide array with period $d = 9\ \mu$m. (b) Coupling coefficient is normalized to the coupling at the central wavelength C_0. (c-e) Evolution of beam intensity and output intensity profiles after 80 mm propagation of a $3\ \mu$m wide input beam for (c) $\lambda_r = 580$ nm, (d) $\lambda_0 = 532$ nm, and (e) $\lambda_b = 490$ nm, which correspond to the points 'c', 'd', and 'e' in (b). Waveguide width is $3\ \mu$m and substrate refractive index is $n_0 = 2.35$ [20].

components $M = 50$ to model accurately the dynamics of beams with broadband spectrum.

When the tilt of beams and waveguides at the input facet is less than the Bragg angle at each wavelength, the beam propagation is primarily characterized by coupling between the fundamental modes of the individual waveguides. Then, beam evolution can be described by the tight-binding equations taking into account periodic waveguide bending [17, 32], which in the linear regime take the form

$$i\frac{d\Psi_n}{dz} + C(\omega)[\Psi_{n+1} + \Psi_{n-1}] = \omega\ddot{x}_0(z)n\Psi_n, \qquad (2)$$

where $\Psi_n(z;\omega)$ are the mode amplitudes, n is the waveguide number, $\omega = 2\pi n_0 d/\lambda$ is the dimensionless frequency, and the dots stand for the derivatives. Coefficient $C(\omega)$ defines a coupling strength between the neighboring waveguides, and it characterizes diffraction strength in a straight waveguide array with $x_0 \equiv 0$ [33, 34]. The coupling coefficient increases with the wavelength [35], and accordingly the beam broadening is substantially larger at long wavelengths, see Figs. 2(b-e).

In order to specially distinguish the effects due to diffraction management, we consider the light propagation in the waveguide arrays with symmetric bending profiles, since asymmetry may introduce other effects due to the modification of refraction, such as beam dragging and steering [36–38]. Specifically, we require that $x_0(z) = f(z - \tilde{z})$ for a given coordinate shift $\tilde{z}$, where function $f(z)$ is symmetric, $f(z) \equiv f(-z)$. Then, by analyzing the plane-wave solutions of Eqs. (2) [17, 20, 32], it can be shown that after the full modulation period ($z \to z + L$) the beam diffraction in the periodically curved waveguide array is the same as in a straight lattice with the effective coupling coefficient

$$C_{\text{eff}}(\omega) = C(\omega)L^{-1}\int_0^L \cos[\omega\dot{x}_0(\zeta)]\,d\zeta. \qquad (3)$$

Therefore, diffraction of multicolor beams is defined by an interplay of the additional bending-induced dispersion introduced through the frequency dependence of the integrand in Eq. (3), and the intrinsic frequency dependence of the coupling coefficient in a straight waveguide array $C(\omega)$. We suggest that spatial evolution of all frequency components can be synchronized allowing for shaping and steering of multicolor beams, when effective coupling remains constant around the central frequency ω_0,

$$\left.\frac{dC_{\text{eff}}(\omega)}{d\omega}\right|_{\omega=\omega_0} = 0, \qquad (4)$$

and we demonstrate below that this condition can be satisfied by introducing special waveguide bending profiles.

3. Self-collimation of white light

First, we demonstrate the possibility for *self-collimation of white-light beams*, where all the wavelength components remain localized despite a nontrivial evolution in the photonic structure. Self-collimation regime is realized when the diffraction is suppressed and the effective coupling coefficient vanishes, $C_{\text{eff}} = 0$. This effect was previously observed for monochromatic beams in arrays with zigzag [3] and sinusoidal [17] bending profiles.

For example, for a sinusoidal modulation function of the form $x_0(z) = A_0\{\cos[2\pi z/L] - 1\}$, which is similar to the one which has been employed to observe experimentally the effect of dynamical localization [17], the self-collimation condition for the frequency ω_0 is realized for the modulation amplitude $A = A_0$ such that $2\pi A_0\omega_0/L = \xi_1$, where $\xi_1 \simeq 2.40$ is the first root of the Bessel function of the first kind of zero order J_0. However, in such structure the condition of zero coupling cannot be satisfied simultaneously with Eq. (4), resulting in strong beam diffraction under frequency detuning from the exact self-collimation value ω_0 by several percent [17], see an example of the beam propagation in a sinusoidally curved waveguide array for different wavelengths in Fig. 3.

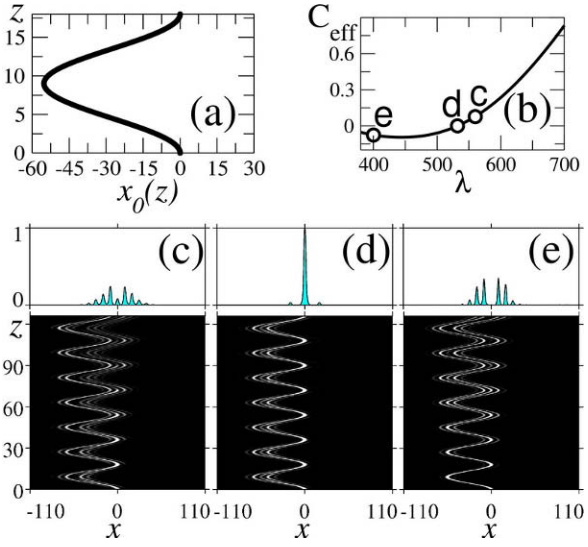


Figure 3. Beam propagation in a sinusoidal waveguide array. (a) Waveguide bending profile with the period $L = 18$ mm and modulation amplitude $A_0 = 27$ μm. (b) Effective coupling normalized to the coupling in the straight array at the central wavelength $C_0 = C(\lambda_0)$. (c-e) Evolution of the beam intensity and output intensity profiles for different wavelengths (c) $\lambda_r = 560$ nm, (d) $\lambda_0 = 532$ nm, and (e) $\lambda_b = 400$ nm, which correspond to points 'c', 'd', and 'e' in (b). Self-collimation takes place for the central wavelength $\lambda_0 = 532$ nm.

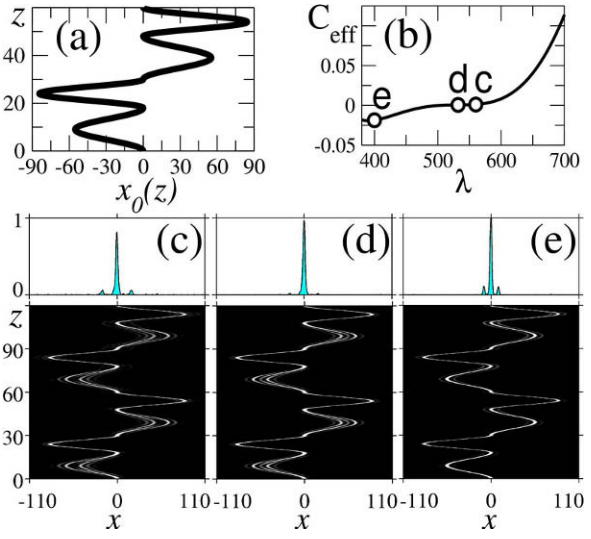


Figure 4. Broadband self-collimation in an optimized modulated waveguide array. (a) Waveguide bending profile with the period $L = 60$ mm and modulation parameters $A_1 = 27$ μm, $A_2 = 42$ μm, $z_0 = 18$ mm. (b) Effective coupling normalized to the coupling in the straight array at the central wavelength $C_0 = C(\lambda_0)$. (c-e) Evolution of the beam intensity and output intensity profiles for different wavelengths (c) $\lambda_r = 560$ nm, (d) $\lambda_0 = 532$ nm, and (e) $\lambda_b = 400$ nm, which correspond to points 'c', 'd', and 'e' in (b).

We find that *broadband diffraction management* becomes possible in hybrid structures with a periodic bending profile that consists of alternating segments [see example in Fig. 4(a)], $x_0(z) = A_1\{\cos[2\pi z/z_0] - 1\}$ for $0 \le z \le z_0$, $x_0(z) = A_2\{\cos[2\pi(z - z_0)/(L/2 - z_0)] - 1\}$ for $z_0 \le z \le L/2$, and $x_0(z) = -x_0(z - L/2)$ for $L/2 \le z \le L$. Effective coupling in such hybrid structure can be calculated analytically, $C_{\text{eff}}(\omega) = C(\omega)2L^{-1}[z_0 J_0(\xi_1) + (L/2 - z_0)J_0(\xi_2)]$, where J_m is the Bessel function of the first kind of the order m, $\xi_1 = 2\pi A_1\omega/z_0$, and $\xi_2 = 2\pi A_2\omega/(L/2 - z_0)$.

We select here a class of symmetric profiles of the waveguide bending to avoid asymmetric beam distortion due to higher-order effects such as third-order diffraction. Additionally, the waveguides are not tilted at the input, i.e. $\dot{x}_0(0) = 0$, in order to suppress excitation of higher-order photonic bands by incident beams inclined by less than the Bragg angle. The effect of Zener tunneling to higher bands [39, 40] and associated scattering losses can be suppressed irrespective of the waveguide tilt inside the photonic structure by selecting sufficiently slow modulation to minimize the curvature $\ddot{x}_0(z)$ and thereby achieve adiabatic beam shaping.

In order to realize broadband self-collimation, we choose the structure parameters such that $\xi_1(\omega_0) = \tilde{\xi}_1$, and $\xi_2(\omega_0) = \tilde{\xi}_2$, where $\tilde{\xi}_2 \simeq 5.52$ is the second root of the function J_0. Then, the self-collimation condition is exactly fulfilled at the central frequency ω_0, $C_{\text{eff}}(\omega_0) = 0$, and simultaneously the condition of wavelength-independent coupling in Eq. (4) is satisfied for the following modulation parameters, $A_1 = [\tilde{\xi}_1\tilde{\xi}_2 J_1(\tilde{\xi}_2)/2\pi(\tilde{\xi}_2 J_1(\tilde{\xi}_2) - \tilde{\xi}_1 J_1(\tilde{\xi}_1))\omega_0]L/2$, $A_2 = -[J_1(\tilde{\xi}_1)/J_1(\tilde{\xi}_2)]A_1$, and $z_0 = 2\pi\omega_0 A_1/\tilde{\xi}_1$. As a result, we obtain an extremely flat coupling curve shown in Fig. 4(b) where the point 'd' corresponds to the central wavelength.

In this hybrid structure not only the first derivative vanishes according to Eq. (4), but the second derivative vanishes as well, $\left|d^2 C_{\text{eff}}(\omega)/d\omega^2\big|_{\omega=\omega_0}\right| \sim \left|\tilde{\xi}_1 J_2(\tilde{\xi}_1)J_1(\tilde{\xi}_2) - \tilde{\xi}_2 J_2(\tilde{\xi}_2)J_1(\tilde{\xi}_1)\right| < 10^{-15}$. As a result, the effective coupling remains close to zero in a very broad spectral region of up to 50% of the central frequency. We note that the modulation period L is a free parameter, and it can always be chosen sufficiently large to avoid scattering losses due to waveguide bending since the maximum waveguide curvature is inversely proportional to the period, $\max|\ddot{x}_0(z)| \sim L^{-1}$. Although the beam evolution inside the array does depend on the wavelength, the incident beam profile is exactly restored after a full modulation period, see examples in Figs. 4(c-e), where results of numerical simulations of Eq. (1) are presented. Self-collimation is preserved even at the red spectral edge,

where coupling length is the shortest and discrete diffraction in the straight array is the strongest [cf. Fig. 4(c) and Fig. 2(c)]. The hybrid structure provides a dramatic improvement in the bandwidth for self-collimation effect compared to the array with a simple sinusoidal modulation, where beams exhibit diffraction under small frequency detuning, see Fig. 3.

4. Broadband diffraction management

We now analyze the conditions for *wavelength-independent normal or anomalous diffraction* that may find applications for reshaping of multicolor beams. In order to reduce the device dimensions, it is desirable to increase the absolute value of the effective coupling and simultaneously satisfy Eq. (4) to achieve broadband diffraction management. We find that Eq. (4) can be satisfied in the two-segment hybrid structure with $z_0 = L/2$ and $A_1 = (\xi/2\pi\omega_0)\,L/2$. Here a set of possible parameter values ξ is determined from the relation $J_0(\xi)/J_1(\xi) = C_0\xi/C_1\omega_0$, where $C_0 = C(\omega_0)$ and $C_1 = dC(\omega)/d\omega|_{\omega=\omega_0}$ characterize dispersion of coupling in a straight array. It is possible to obtain both normal and anomalous diffraction regimes for normally incident beams, corresponding to positive and negative effective couplings $C_{\text{eff}}(\omega_0) = C_0 J_0(\xi)$ depending on the chosen value of ξ. For example, for the waveguide array shown in Fig. 2, at the central frequency $\omega_0 = 250$ [corresponding wavelength is $\lambda_0 = 532$ nm] calculated numerically coupling parameters are $C_0 \simeq 0.13$ mm^{-1} and $C_1 \simeq -0.0021$ mm^{-1}. Then, constant positive coupling around the central frequency $C_{\text{eff}}(\omega_0) \simeq 0.25C_0$ is realized for $\xi \simeq 6.47$ and constant negative coupling $C_{\text{eff}}(\omega_0) \simeq -0.25C_0$ for $\xi \simeq 2.97$.

We perform a comprehensive analytical and numerical analysis, and find that a hybrid structure with bending profile consisting of one straight (i.e $A_1 \equiv 0$) and one sinusoidal segment can provide considerably improved performance if $\omega_0 C_1/C_0 > \xi_{cr} J_1(\xi_{cr})/J_0(\xi_{cr})$, where value $\xi_{cr} \simeq 5.84$ is found from the equation $[J_1(\xi_{cr}) + \xi_{cr}[J_0(\xi_{cr}) - J_2(\xi_{cr})]/2][J_0(\xi_{cr}) - 1] + \xi_{cr} J_1^2(\xi_{cr}) = 0$. Under such conditions, larger values of positive effective coupling can be obtained in a hybrid structure with $A_1 \equiv 0$, $A_2 = [C_1 C_{\text{eff}}(\omega_0)/2\pi C_0^2 J_1(\tilde{\xi}_2)]L/2$, $z_0 = [C_{\text{eff}}(\omega_0)/C_0]L/2$. In this structure, the effective coupling at central frequency is $C_{\text{eff}}(\omega_0) = \tilde{\xi}_2 C_0^2 J_1(\tilde{\xi}_2)/[\tilde{\xi}_2 C_0 J_1(\tilde{\xi}_2) + \omega_0 C_1]$.

Example of a hybrid structure which provides strong wavelength-independent diffraction is shown in Fig. 5(a), and the corresponding effective coupling is plotted in Fig. 5(b). The diffraction rate in this optimized structure is almost the same in a broad spectral region, see examples

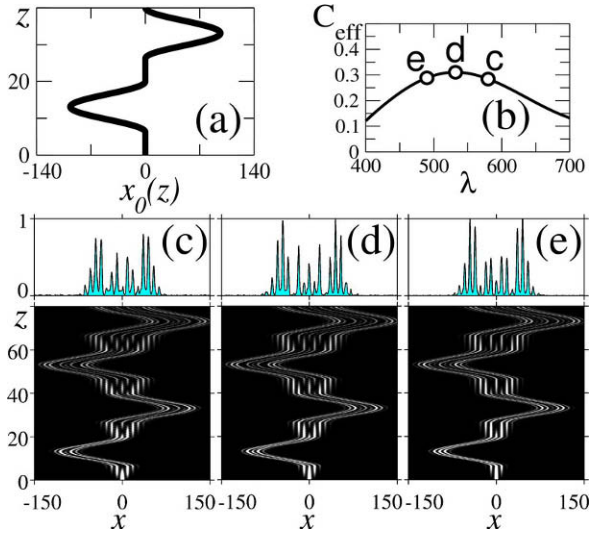


Figure 5. Wavelength-independent diffraction in an optimized periodically curved waveguide array. (a) Waveguide bending profile with the period $L = 40$ mm and (b) corresponding effective coupling normalized to the coupling in the straight array at the central wavelength $C_0 = C(\lambda_0)$. (c-e) Evolution of beam intensity and output intensity profiles after propagation of two full periods for the wavelengths (c) $\lambda_r = 580$ nm, (d) $\lambda_0 = 532$ nm, and (e) $\lambda_b = 490$ nm, which correspond to points 'c', 'd', and 'e' in (b) [20].

for three wavelengths in Figs. 5(c-e). We note that the output beam profiles at these wavelengths are substantially different after the same propagation length in the straight waveguide array, as shown in Figs. 2(c-e).

5. Multicolor Talbot effect

As one of the applications of the broadband diffraction management we consider a *multicolor Talbot effect* which allows to manipulate polychromatic light patterns. The Talbot effect, when any periodical monochromatic light pattern reappears upon propagation at certain equally spaced distances, has been known since the famous discovery in 1836 [41]. It was recently shown that the Talbot effect is also possible in discrete systems for certain periodic input patterns [35]. For example, for the monochromatic periodic input pattern of the form $\{1, 0, 0, 1, 0, 0, \ldots\}$, Talbot revivals take place at the distance $L_T^{(1)} = (2\pi/3)[1/C(\omega)]$, see Fig. 6(a).

Period of the discrete Talbot effect in the waveguide array is inversely proportional to the coupling coefficient $C(\omega)$, which strongly depends on frequency, see Fig. 2(b). Therefore, for each specific frequency Talbot recurrences occur at different distances [35], and periodic intensity revivals disappear for the multicolor input, see Fig. 6(b).

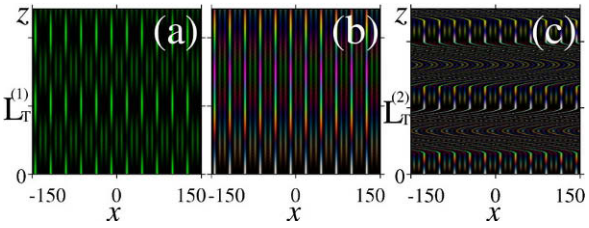


Figure 6. (a) Monochromatic Talbot effect in the straight waveguide array shown in Fig. 2(a): periodic intensity revivals every $L_T^{(1)} = 16.5$ mm of the propagation distance for the input pattern $\{1,0,0,1,0,0,\ldots\}$ and the wavelength $\lambda_0 = 532$ nm. (b) Disappearance of the Talbot carpet in the straight array when input consists of three components with equal intensities and different wavelengths $\lambda_r = 580$ nm [red-shifted], $\lambda_0 = 532$ nm [green], and $\lambda_b = 490$ nm [blue-shifted]. (c) Multicolor Talbot effect in the optimized structure with wavelength-independent diffraction [see Fig. 5.] Half of the bending period $L/2 = L_T^{(2)} = 53.2$ mm is equal to the Talbot distance for the corresponding effective coupling length [20].

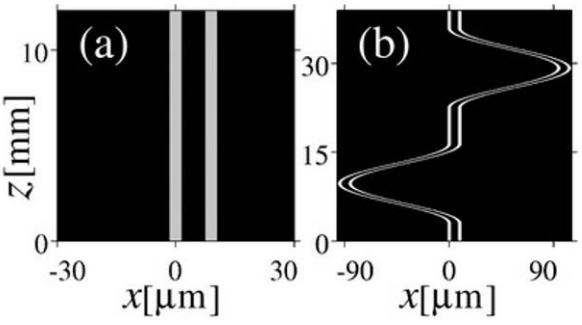


Figure 7. (a) Conventional directional coupler composed of two evanescently coupled straight waveguides. (b) Polychromatic light coupler with specially designed bending of the waveguide axes. Waveguide width and separation between waveguide axes are 3 μm and 9 μm, respectively. Refractive index contrast is $\Delta n = 8 \times 10^{-4}$, and $n_0 = 2.35$.

Multicolor Talbot effect is also not possible in free space where revival period is proportional to frequency. Most remarkably, we demonstrate that multicolor discrete Talbot effect can be observed in optimized modulated waveguide arrays with wavelength-independent diffraction, see Fig. 6(c). In this example, we use the shape of structure with constant positive diffraction shown in Fig. 5, and choose half of the bending period to be equal to the period of the Talbot recurrences for the corresponding effective coupling in this structure, $L_T^{(2)} = (2\pi/3)[1/C_{\text{eff}}(\omega)]$.

6. Directional coupler for white light

Directional waveguide coupler is the device which utilizes light tunneling between two optical waveguides placed in close proximity to each other, as schematically shown in Fig. 7(a). In the linear regime, as light propagates in a directional coupler made of straight identical waveguides, the power is periodically exchanged between the two waveguides [42] with the period which is defined by the coupling length, $Z_c = \pi/[2C(\lambda)]$, where $C(\lambda)$ is the coupling coefficient. Then, the complete power transfer from one waveguide at the input to the other waveguide at the output can be realized by choosing the device length as an odd number of coupling lengths.

Over the last decades, nonlinear waveguide couplers, first introduced by Jensen [42] and Maier [43], have attracted a great deal of attention as major candidates for creation of ultra-fast all-optical switches, as at high input powers, intensity-dependent change of the refractive index through optical nonlinearity creates detuning between the waveguides which can suppress power transfer between coupler arms, such that light remains in the input waveguide. Since the first experimental demonstration of a subpicosecond nonlinear coupler switch in a dual-core fiber [44], various aspects of switching in different coupler configurations has been extensively analyzed [45–49].

However, conventional coupler can only perform switching of signals with rather limited spectral bandwidth, because the coupling length depends on optical frequency [see Fig. 2(b)], resulting in strong separation of different frequency components between the waveguides, as shown in Figs. 8(a) and (c).

We find that the operating bandwidth of conventional coupler consisting of straight parallel waveguides [Fig. 7(a)] can be improved dramatically by introducing special bending of waveguide axes in the propagation direction as illustrated in Fig. 7(b). The effect of axes bending on light propagation in *two* coupled waveguides can be approximately described in terms of the effective coupling coefficient C_{eff}, which takes the same form as for the infinite array of coupled optical waveguides [50], see Eq. (3). Similar to the method used in Sec. 4, we find that wavelength-insensitive effective coupling around the central wavelength λ_0 can be realized in a hybrid structure consisting of alternating straight and sinusoidal segments [see Fig. 7(b)], $x_0(z) = 0$ for $0 \le z \le z_0$, $x_0(z) = A\{\cos[2\pi(z-z_0)/(z_1-z_0)] - 1\}$ for $z_0 \le z \le z_1$, $x_0(z) = 0$ for $z_1 \le z \le L/2$, and $x_0(z) = -x_0(z - L/2)$ for $L/2 \le z \le L$. We set $A = \tilde{\xi}_2(z_1 - z_0)\lambda_0(4\pi^2 n_0 a)^{-1}$ and $z_1 = L/2 - z_0$. Effective coupling in this structure is $C_{\text{eff}}(\lambda) = C(\lambda)L^{-1}[4z_0 + (L - 4z_0)J_0(\tilde{\xi}_2\lambda_0/\lambda)]$, and the condition of wavelength-insensitive coupling (4) is satisfied for $z_0 = (L/4)\left[1 - C_1(\tilde{\xi}_2 J_1(\tilde{\xi}_2)C_0)^{-1}\right]^{-1}$. Here the coefficients $C_0 = C(\lambda_0)$ and $C_1 = \lambda_0\, dC(\lambda)/d\lambda|_{\lambda=\lambda_0}$ characterize coupling dispersion for straight waveguides. In numer-

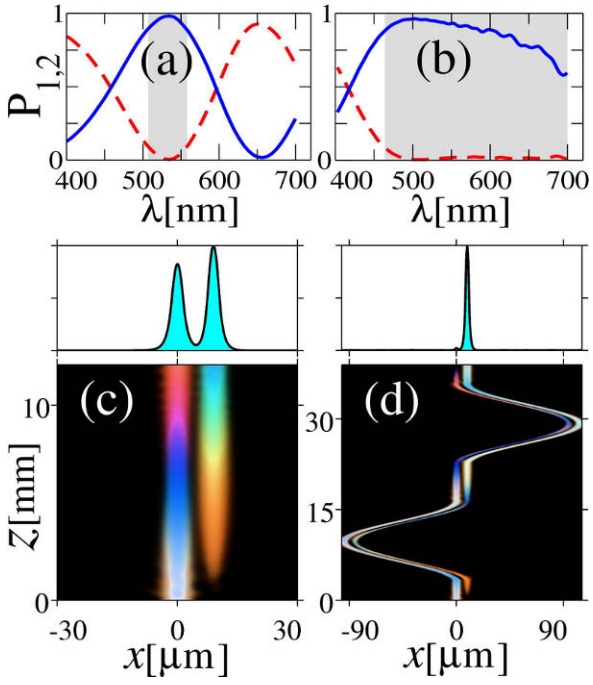


Figure 8. (a,b) Wavelength dependence of linear transmission of straight and optimized curved couplers, respectively. Shown are output powers in the left (dashed curve, P_1) and right (solid curve, P_2) coupler arms when light is launched into the left coupler arm at the input. Shading marks spectral regions where the switching ratio P_2/P_1 is larger than 10. (c,d) Evolution of polychromatic light with flat spectrum covering $450-700$ nm in the straight and in the optimized curved structures, respectively. Top panels in (c) and (d) show the total intensity distributions at the output [22].

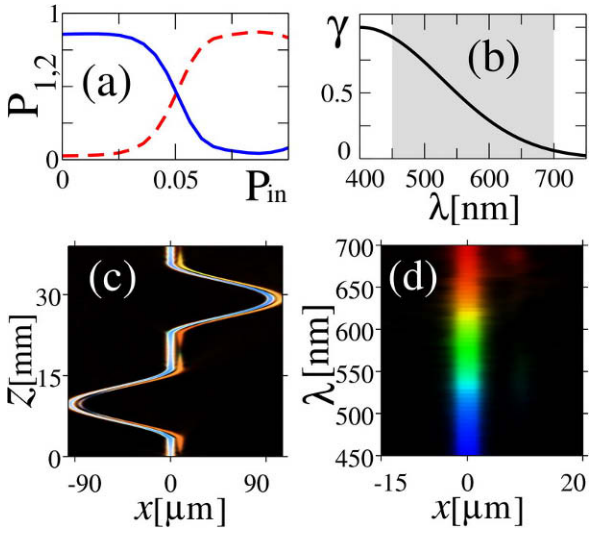


Figure 9. Nonlinear switching of polychromatic light. (a) Power distribution at the output ports of the coupler as a function of the input power. Polychromatic input is the same as in Figs. 8(c) and 8(d). Solid and dashed curves show power in the left (P_1) and in the right (P_2) output coupler ports, respectively. (b) Sensitivity function γ describing wavelength-dispersion of the nonlinear response. (c,d) Propagation dynamics and output spectrum, respectively, in the nonlinear switched state realized at the total input power $P_{in} = 0.085$. Nonlinear coefficient is $\alpha = 10$ [22].

ical simulations, we choose $\lambda_0 = 532$ nm, and find the coupling dispersion for waveguides shown in Fig. 7(a) as $C_0 \simeq 0.13$ mm^{-1} and $C_1 \simeq 0.52$ mm^{-1}. Then, we calculate the optimal parameters of the curved coupler, and obtain almost constant coupling $C_{\text{eff}}(\lambda \simeq \lambda_0) \simeq 0.31 C_0$ in a broad spectral region.

Such optimized curved coupler can be used to collectively switch all spectral components around the central wavelength λ_0 from one input waveguide to the other waveguide at the output if the device length is matched to the effective coupling length, i.e. $L = \pi/[2C_{\text{eff}}(\lambda_0)] \simeq 39$ mm. We then perform numerical simulations based on full model Eqs. (1) and confirm that the proposed coupler structure indeed exhibits extremely efficient switching into the crossed state simultaneously in a very broad spectral region of about $450-700$ nm, which covers almost the entire visible, see Figs. 8(b) and 8(d). This is in a sharp contrast to the conventional straight coupler [Figs. 8(a) and 8(c)] that can only operate in the spectral region of $\sim 510-560$ nm, which is about five time less than for the proposed curved coupler. We note that slight decrease of the output power at the red edge of the spectrum for the curved coupler [Fig. 8(b)] is caused by the radiation at the waveguide bends [50], but such losses do not affect the broadband switching behavior.

At high input powers, nonlinear change of the refractive index modifies waveguide propagation constant and decouples waveguides from each other similar to other nonlinear coupler structures studied before [42, 44, 51]. This causes switching from crossed state into the parallel state as shown in Figs. 9(a), 9(c) and 9(d). Remarkably, nonlinear switching also takes place in a very broad spectral region $\sim 450-700$ nm, which enables the coupler to act as an all-optical digital switch for polychromatic light. In our simulations, we consider the case of a photorefractive medium such as $LiNbO_3$ where optical waveguides of arbitrary configuration can be fabricated by titanium indiffusion [52, 53]. In the $LiNbO_3$ waveguide arrays, the photovoltaic nonlinearity arises due to charge excitations by light absorption and corresponding separation of these charges due to diffusion. The spectral response of this type of nonlinearity depends on the crystal doping and stoichiometry, and it may vary from crystal to crystal. In general light sensitivity appears in a wide spectral range with a maximum for the

blue spectral components [54], but the sensitivity extends also in the near infra-red region [55]. We approximate the photosensitivity dependence by a Gaussian function $\gamma(\lambda) = \exp[-\log(2)(\lambda - \lambda_b)^2/\lambda_w^2]$, where $\lambda_b = 400$ nm and $\lambda_w = 150$ nm [Fig. 9(b)]. We have checked that the switching behavior of the coupler remains essentially the same for a range of other values of λ_w, which primarily affect the quantitative characteristics such as the switching power.

7. Periodically curved two-dimensional waveguide arrays

The recent advances in waveguide fabrication with direct femtosecond laser writing [26–29] make it possible to realize structures of arbitrary two-dimensional geometry. It is therefore important to extend the concept of polychromatic light diffraction management to the case of two-dimensional structures. As an example, we consider a hexagonal modulated photonic lattice, [see Fig. 10(a)], where the waveguide axes are periodically curved in the longitudinal propagation direction [see an example in Fig. 10(b)]. We take into account the mode coupling between the neighboring waveguides, defined by the real-valued coefficients C_1, C_2, and C_3 which characterize diffraction in a straight hexagonal waveguide array [see Fig. 10(c)]. Using the approach developed for one-dimensional periodically curved waveguide arrays which has been outlined in Sec. 2, we show that after the full bending period [$z \to z+L$], the beam diffraction in the periodically curved hexagonal waveguide array is the same as in a straight hexagonal waveguide array with the effective coupling coefficients [21]

$$C_{1\text{eff}} = C_1 L^{-1} \int_0^L \cos[\omega \dot{x}_0(\zeta)]\, d\zeta, \quad (5)$$

$$C_{2\text{eff}} = C_2 L^{-1} \int_0^L \cos\left[\frac{\omega}{2}\dot{x}_0(\zeta) + \frac{\sqrt{3}}{2}\omega \dot{y}_0(\zeta)\right] d\zeta, \quad (6)$$

$$C_{3\text{eff}} = C_3 L^{-1} \int_0^L \cos\left[\frac{\omega}{2}\dot{x}_0(\zeta) - \frac{\sqrt{3}}{2}\omega \dot{y}_0(\zeta)\right] d\zeta, \quad (7)$$

where the two functions $x_0(z) \equiv x_0(z+L)$ and $y_0(z) \equiv y_0(z+L)$ define periodic axes bending in the two-dimensional lattice.

We note that the values of the effective coupling coefficients depend not only on the specific bending profile $x_0(z)$ and $y_0(z)$, but also on the frequency ω, similar to the bending-induced coupling dispersion which appears in one-dimensional periodically curved waveguide arrays [20]. This means that different frequency components may experience very different types of diffraction in *the same* physical structure. This feature provides unique opportunities for the control and reshaping of polychromatic light beams in two dimensional photonic lattices. To illustrate this effect, we consider the propagation of light beams of different wavelengths in the same modulated hexagonal lattice with a simple sinusoidal bending profile in the $x-z$ plane: $x_0(z) = A_1\{\cos[4\pi z/L] - 1\}$ for $0 \le z \le L/2$, $x_0(z) = -x_0(z - L/2)$ for $L/2 \le z \le L$, and $y_0(z) \equiv 0$.

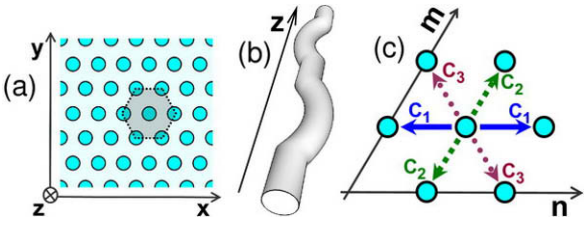


Figure 10. Sketch of modulated hexagonal photonic lattice. (a) Transverse lattice cross-section. Shading marks the unit cell, each lattice site has six nearest neighbors. (b) Schematic of the individual waveguide with the axis periodically curved in the z-direction. (c) Couplings between the nearest neighbours in the hexagonal lattice. Lattice sites are numbered along the n and m-axes [21].

From the Eqs. (5)-(7) it follows that for the light wavelength such that the normalized frequency is $\omega_1 = \tilde{\xi}_1 L/2\pi A_1$, the diagonal couplings vanish, $C_{2\text{eff}} = C_{3\text{eff}} = 0$, while the horizontal coupling is reduced, $C_{1\text{eff}} = C_1 J_0(2\tilde{\xi}_1) \simeq -0.24 C_1$. Then, the beam at this wavelength will experience a *one dimensional* diffraction, as shown in Fig. 11(a). In this example, some weak coupling to upper and lower lattice rows also takes place. This is due to high-order coupling and increased scattering effects, which are stronger for long wavelengths. We expect that the high-order coupling can be suppressed in modulated lattices by a special design of waveguide bending profiles, similar to results demonstrated for one-dimensional waveguide arrays [56].

On the other hand, for the frequency $\omega_2 = \tilde{\xi} L/2\pi A_1$, where $\tilde{\xi} \simeq 2.61$ is determined from the equation $J_0(\tilde{\xi}) = J_0(2\tilde{\xi})$, all three couplings are reduced simultaneously by the same factor $C_{1,2,3\text{eff}} = C_{1,2,3} J_0(\tilde{\xi}) \simeq -0.10 C_{1,2,3}$, and the symmetry of the original hexagonal lattice is exactly preserved, see Fig. 11(b) where the beam experiences reduced *hexagonal* diffraction.

For the frequency $\omega_3 = \tilde{\xi}_2 L/4\pi A_1$, the horizontal coupling is canceled $C_{1\text{eff}} = 0$, while the diagonal couplings are reduced symmetrically $C_{2,3\text{eff}} = C_{2,3} J_0(\tilde{\xi}_2/2) \simeq -0.17 C_{2,3}$. Accordingly, the beam at this frequency experiences a *rectangular* diffraction [see Fig. 11(c)]. Indeed, despite the nontrivial beam evolution in between the periods, the diffraction pattern after each bending period is similar to

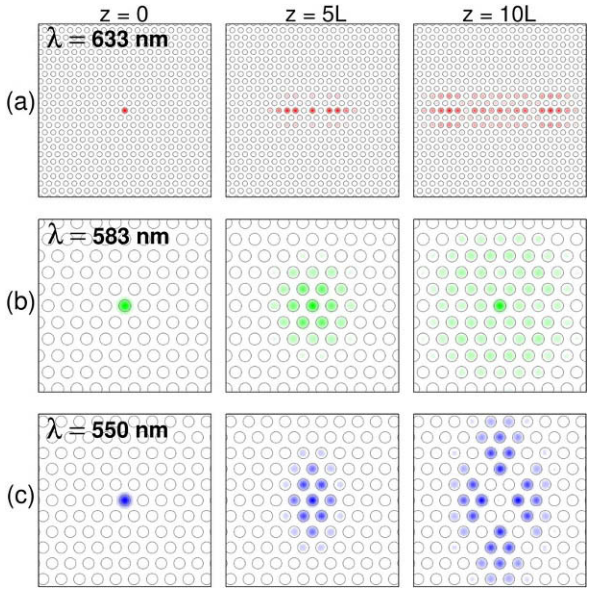


Figure 11. Examples of different diffraction patterns in *the same* modulated hexagonal lattice. (a) One-dimensional diffraction at the wavelength $\lambda = 633$ nm. (b) Hexagonal diffraction at the wavelength $\lambda = 583$ nm. (c) Rectangular diffraction at the wavelength $\lambda = 550$ nm [21].

diffraction patterns which are characteristic of the discrete diffraction in square and rectangular photonic lattices, where each lattice site is coupled to four nearest neighbors.

8. Conclusions

We have presented an overview of the basic theoretical studies of spatio-spectral control of polychromatic light in periodically modulated photonic lattices. We have demonstrated that the wavelength dispersion can be engineered in optimized arrays of curved optical waveguides allowing an efficient diffraction management of polychromatic light beams, and realization of multicolor Talbot effect for polychromatic light patterns, which is not possible in free space or in conventional photonic lattices. We have also demonstrated that the nonlinear interaction of different spectral components in specially designed periodically curved directional coupler enables broadband all-optical switching of polychromatic light. Our simulations indicate that these theoretically predicted effects can be observed experimentally in a variety of photonic structures. We anticipate that suggested approaches for the switching and control of polychromatic light beams may also find applications for tunable shaping of optical pulses with ultra-broad spectrum, offering additional functionality for broadband optical systems and devices.

Acknowledgements

We would like to thank our collaborators and colleagues for their substantial and valuable contributions to the results summarized in this review paper. Especially, we are indebted to W. Krolikowski, D. Neshev, S. Nolte, T. Pertsch, A. Szameit, and A. Tünnermann. The work has been supported by the Australian Research Council through Discovery and Centre of Excellence Projects.

References

[1] J.D. Joannopoulos, R.D. Meade, J.N. Winn, Photonic Crystals: Molding the Flow of Light (Princeton University Press, Princeton, 1995)
[2] P.St.J. Russell, T.A. Birks, F.D. Lloyd Lucas, in Confined Electrons and Photons, E. Burstein, C. Weisbuch, eds., (Plenum, New York, 1995) 585
[3] H.S. Eisenberg, Y. Silberberg, R. Morandotti, J.S. Aitchison, Phys. Rev. Lett. 85, 1863 (2000)
[4] Y.V. Kartashov, L. Torner, V.A. Vysloukh, Opt. Express 13, 4244 (2005)
[5] P.T. Rakich et al., Nat. Mater. 5, 93 (2006)
[6] T. Pertsch, T. Zentgraf, U. Peschel, A. Brauer, F. Lederer, Phys. Rev. Lett. 88, 093901 (2002)
[7] P.V. Parimi, W.T.T. Lu, P. Vodo, S. Sridhar, Nature 426, 404 (2003)
[8] Z.L. Lu et al., Phys. Rev. Lett. 95, 153901 (2005)
[9] J.K. Ranka, R.S. Windeler, A.J. Stentz, Opt. Lett. 25, 25 (2000)
[10] P.St.J. Russell, Science 299, 358 (2003)
[11] J.M. Dudley, G. Genty, S. Coen, Rev. Mod. Phys. 78, 1135 (2006)
[12] T. Udem, R. Holzwarth, T.W. Hansch, Nature 416, 233 (2002)
[13] A.M. Zheltikov, Usp. Fiz. Nauk 176, 623 (2006) (in Russian) [Phys. Usp. 49, 605 (2006)].
[14] B. Povazay et al., Opt. Lett. 27, 1800 (2002)
[15] M.H. Qi et al., Nature 429, 538 (2004)
[16] H. Kosaka et al., J. Lightwave Technol. 17, 2032 (1999)
[17] S. Longhi et al., Phys. Rev. Lett. 96, 243901 (2006)
[18] L.J. Wu, M. Mazilu, T. Karle, T.F. Krauss, IEEE J. Quantum Electron. 38, 915 (2002)
[19] J. Wan, M. Laforest, C.M. de Sterke, M.M. Dignam, Opt. Commun. 247, 353 (2005)
[20] I.L. Garanovich, A.A. Sukhorukov, Yu.S. Kivshar, Phys. Rev. E 74, 066609 (2006)

[21] I.L. Garanovich et al., Opt. Express 15, 9737 (2007)
[22] I.L. Garanovich, A.A. Sukhorukov, Opt. Lett. 32, 475 (2007)
[23] A.A. Sukhorukov et al., Opt. Express 14, 11265 (2006)
[24] D.N. Neshev et al., Phys. Rev. Lett. 99, 123901 (2007)
[25] A.A. Sukhorukov, D.N. Neshev, Yu.S. Kivshar, Opt. Express 15, 13058 (2007)
[26] S. Nolte, M. Will, J. Burghoff, A. Tuennermann, Appl. Phys. A 77, 109 (2003)
[27] T. Pertsch et al., Opt. Lett. 29, 468 (2004)
[28] A. Szameit et al., Opt. Express 13, 10552 (2005)
[29] A. Szameit et al., Appl. Phys. B 82, 507 (2006)
[30] M. Mitchell, M. Segev, Nature 387, 880 (1997)
[31] H. Buljan, T. Schwartz, M. Segev, M. Soljacic, D.N. Christodoulides, J. Opt. Soc. Am. B 21, 397 (2004)
[32] S. Longhi, Opt. Lett. 30, 2137 (2005)
[33] A.L. Jones, J. Opt. Soc. Am. 55, 261 (1965)
[34] S. Somekh, E. Garmire, A. Yariv, H.L. Garvin, R.G. Hunsperger, Appl. Phys. Lett. 22, 46 (1973)
[35] R. Iwanow et al., Phys. Rev. Lett. 95, 053902 (2005)
[36] Y.V. Kartashov, L. Torner, D.N. Christodoulides, Opt. Lett. 30, 1378 (2005)
[37] I.L. Garanovich, A.A. Sukhorukov, Yu.S. Kivshar, Opt. Express 13, 5704 (2005)
[38] C.R. Rosberg et al., Opt. Lett. 31, 1498 (2006)
[39] C. Zener, Proc. R. Soc. London A 145, 523 (1934)
[40] H. Trompeter et al., Phys. Rev. Lett. 96, 023901 (2006)
[41] H.F. Talbot, Phil. Mag. 9, 401 (1836)
[42] S.M. Jensen, IEEE Trans. Microw. Theory Tech. MTT-30, 1568 (1982)
[43] A.A. Maier, Kvantov. Elektron. 9, 2296 (1982) (in Russian) [Quantum Electron. 12, 1490 (1982)].
[44] S.R. Friberg et al., Appl. Phys. Lett. 51, 1135 (1987)
[45] V. Leutheuser, U. Langbein, F. Lederer, Opt. Commun. 75, 251 (1990)
[46] G. Assanto, G. Stegeman, M. Sheik-Bahae, E. Van Stryland, Appl. Phys. Lett. 62, 1323 (1993)
[47] M.A. Karpierz, T.R. Wolinski, Pure Appl. Opt. 4, 61 (1995)
[48] I.M. Skinner, G.D. Peng, B.A. Malomed, P.L. Chu, Opt. Commun. 113, 493 (1995)
[49] A. Betlej et al., Opt. Lett. 31, 1480 (2006)
[50] S. Longhi, Phys. Rev. A 71, 065801 (2005)
[51] R.V. Mendes, Opt. Commun. 232, 425 (2004)
[52] F. Chen et al., Opt. Express 13, 4314 (2005)
[53] M. Matuszewski et al., Opt. Express 14, 254 (2006)
[54] R.R. Shah, D.M. Kim, T.A. Rabson, F.K. Tittel, J. Appl. Phys. 47, 5421 (1976)
[55] F. Jermann, M. Simon, E. Kratzig, J. Opt. Soc. Am. B 12, 2066 (1995)
[56] R. Iyer, J.S. Aitchison, J. Wan, M.M. Dignam, C.M. de Sterke, Opt. Express 15, 3212 (2007)